MONTHLY WEATHER REVIEW

VOLUME 94, NUMBER 4

APRIL 1966

ATMOSPHERIC MOTIONS FROM SODIUM CLOUD DRIFTS AT FOUR LOCATIONS

ADAM KOCHANSKI

Environmental Science Services Administration, Washington, D.C.

ABSTRACT

Atmospheric motions from 54 sodium cloud firings are examined in the 80–200-km. height region. To gain an insight into various types of motion that are presumably present in the total observed wind, an oscillatory component assigned to internal gravity waves, and the residual motion containing tides and prevailing wind, are studied. Data from apparent movements of ionospheric irregularities seem, in many respects, consistent with sodium drift measurements and are utilized to estimate the prevailing wind and the 24-hr. and 12-hr. periodic variations. Only inferential results can be obtained from many parts of this analysis, but there is a strong suggestion that a slowly varying prevailing wind has a substantial role in these motions; the magnitude of this wind appears to be 45 m./sec. in the 100–115-km. layer and 65 m./sec. near 160 km. At three stations located within the 30°–40° N. latitudes, both the observed and the derived motions are very similar, as if a well organized circulation existed at all heights from 80 to 180 km. Fort Churchill data indicate that farther north this circulation may be considerably stronger.

1. INTRODUCTION

Continuing an earlier work on sodium cloud drifts [10], an expanded analysis of atmospheric motions in the lower thermosphere has been carried out with data from four different locations. The investigation has been primarily concerned with identification of various types of motion that are hidden in the observed sodium cloud drifts. Important inferences can be drawn from such analysis, including energy transfer from the lower to the higher atmosphere. There is strong evidence, for example, that the system of internal gravity waves is depositing a substantial portion of its energy at higher elevations and Hines [8] estimated that heating rates from this source alone amount to 30°K. per day at 110 km. and 100°K. per day at 140 km. Little can be said about the behavior of atmospheric tides above 100 km., but if tides attenuate with height, an additional amount of energy would be deposited in the atmosphere.

The technique of drift measurements is well known and a brief description will suffice to outline the quality of the data used in the present paper. Chemoluminous trails lasting 2 to 10 min. are produced in the 70–200-km. height region by releasing from rockets certain, mostly metallic, compounds. Several photographs of trails are taken during their lifetime and motions of characteristic points are computed and averaged. Up to 150 km., claimed RMS accuracy of drift measurements is 3 m./sec., and the accuracy of height determination 100 m. By far the most popular experiments are sodium releases which have provided about 80 percent of the presently available data, and releases of aluminum compounds that emit glow at twilight and also in complete darkness (about 15 percent).

Sodium experiments can be performed only during morning and evening twilight hours and are inadequate for studying such problems as, for example, tidal motions. Sodium cloud firings began in 1956 [12], but only a few soundings were added each year and these data will likely remain, for a long time, insufficient for a rigorous statistical treatment. Closely spaced nighttime experiments utilizing aluminum compounds are now possible, but presently available data cover only parts of two nights, with four experiments each, at Eglin, Fla.

For brevity, the term "sodium clouds" will be used throughout this paper.

2. DATA SOURCES

In an earlier work [10] we utilized only 25 sodium cloud profiles, mostly from Wallops Island. Available for the present study were 54 profiles distributed among four locations as indicated below:

Number of firings	*Location*		*Sources*
23	Eglin	30° N., 86.5° W.	[18]
23	Wallops Island	38° N., 75.5° W.	[5, 14]
5	Sardinia	39.5° N., 9.5° E.	[3]
3	Fort Churchill	59° N., 92.5° W.	[14]

The best overall data cover, viz. 49–54 soundings, was for the 102–112-km. layer. The number of observations decreased both below and above this region, and was 30 at 130 km., 21 at 160 km., and 8 at 180 km. Most of the data for Eglin were limited to the 95–130-km. layer. Since sodium cloud experiments are being continued, it is pertinent to list the dates of the latest soundings utilized in the present study: May 21, 1963 for Eglin, May 24, 1963 for Wallops Island, September 8, 1963 for Sardinia, and May 22, 1963 for Fort Churchill. We were unable to use six firings from Hammaguir, Algeria, because published data [2] contained only the direction of the drifts.

3. TYPES OF MOTION

It can be hypothesized that the observed motion revealed by sodium cloud experiments is a sum of three independent types of motion, viz.: (1) internal gravity waves postulated by Hines [6]; (2) atmospheric tides; (3) drift, defined as a slowly varying component similar to the "prevailing wind" from the radio meteor winds region. Accepting this assumption, one can remove from the observed motion the oscillating component due to internal gravity waves, and treat the residual motion as the sum of drift and tidal components. It should be emphasized that this is only one of several possible approaches. Rosenberg and Justus [20], for example, assigned most of the motion observed during two nighttime series to semidiurnal tidal waves, leaving only small residuals to account for drift and short-period gravity waves.

In the present study we have adopted a previously introduced technique [10] which assumes the presence of an appreciable gravity wave component. The observed motion is resolved into a term **W** which represents the amplitude of the wave motion, and the residual term **R** which is the sum of the prevailing drift and tidal components. Figure 1 outlines this technique and illustrates the results for one sounding. From the observed speed profile we select maxima and minima of velocity, labeled A, B, C, etc. The vectors of the observed wind $\mathbf{V_A}$, $\mathbf{V_B}$, $\mathbf{V_C}$, etc., are then plotted as shown in the upper part of figure 1. Vector **W** represents the amplitude of the wave motion, where $+\mathbf{W}$ and $-\mathbf{W}$ for the adjacent layers are equal in magnitude and opposite in direction. Vector **R** is the residual term.

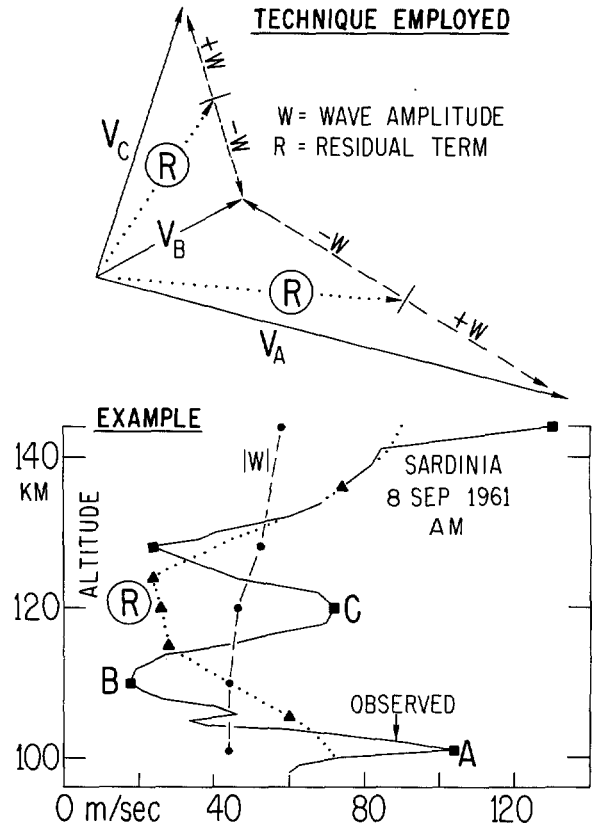

FIGURE 1.—Vectorial resolution technique and its results in the case of one sodium wind profile from Sardinia.

Sketched in the lower part of figure 1 are derived vertical profiles of $|W|$ and R; direction profiles are not shown. Inherent in this resolution technique is the property of **W** and **R** to retain certain characteristics of the observed motion. For example, vector $+\mathbf{W}$ is forced to have direction similar to that of the adjacent velocity maximum of the observed wind, such as $\mathbf{V_A}$, or $\mathbf{V_C}$ in figure 1. A very close similarity found between vectorial averages of **R** and those of the observed wind will be discussed later.

This technique yields consistent results that can be interpreted physically, but relies on subjective identification of the vertical wavelength of velocity oscillations. As pointed out by Hines [8], it may underestimate the appearance of wave motion at heights greater than, say, 140 km. The theory of the internal gravity waves [6, 7] specifies the shortest permissible vertical half wavelengths, $\lambda_z/2$, but sets no upper limits for this parameter. The lower limit for $\lambda_z/2$ is, for example, 14 km. at 140 km. and 40 km. at the height of 180 km. Actually existing prevailing modes may have much greater wavelengths than quoted above, and they may not be detectable on sodium cloud profiles. The nature of the observed wind makes it still more complicated: a "quiescent region" exists between 140 and 200 km. where the direction of the observed wind changes little with elevation and where over very large vertical intervals speed oscillations are

not apparent. In many individual cases one must be guided by the reasonableness of **W** and **R** profiles, and the identification of wave motion becomes truly subjective. In the present paper we attempted to remedy this shortcoming by including, at higher elevations, even doubtful cases of wave motion.

The residual term **R** obtained by this technique is essentially a wind smoothed over vertical intervals of $\lambda_z/2$, which happens to be about 6 km. at heights from 80 to 120 km. and grows with elevation. In profiles of **R**, the extremes of speed and direction present in the observed wind are removed. In individual profiles the values of **R** at any level depart widely from those of the observed wind. It is found, however, that vectorial averages of **R** are very close indeed to the averages of the observed wind. This is because the wave motion adds to and subtracts from **R** in a nearly random manner, and its positive and negative contributions tend to cancel out. Thus in vectorial averages the directions of **R** and of the observed wind are nearly identical, while the mean speed of **R** is only 6 to 14 percent lower than that of the observed wind. Similar considerations apply to contributions of tidal motions; if one averages the a.m. and p.m. values for **R**, the contributions of the diurnal tides cancel out, and vector **R** is simply the sum of drift and a component due to semidiurnal tides.

It should be kept in mind that the contribution of a gravity wave to the total observed wind is a vector that varies quasi-sinusoidally over the interval λ_z, from $+\mathbf{W}$ through zero velocity to $-\mathbf{W}$. Thus in the vertical plane the average contribution of the wave motion should be $2W/\pi$; this is confirmed by the RMS evaluation from individual cases. Using scalar quantities V, R, and W, we find that

$$[(\sum V^2-\sum R^2)/n]^{1/2}=0.67W\cong 2W/\pi$$

For horizontal planes similar evaluation yields a value of $1.16(2W/\pi)$, i.e., the term $(V^2-R^2)^{1/2}$ again suggests a slightly larger contribution of the wave motion than expected from a random distribution of wave vectors at any level. One of the possible explanations is that wave motion and the residual motion are not strictly independent. As shown in section 6, the wave motion is polarized and probably correlated with the prevailing wind which, in turn, enters into the residual motion **R**. It should be also kept in mind that the factor 1.16 comes from computations that encompass values from ten levels (95, 100, 105 km., . . ., 140 km.); considering single levels we find that this factor can range from 1.59 to 0.65, but values smaller than 1.00 appear in only 18 percent of the cases.

4. THE OBSERVED MOTIONS

The observed motions revealed by sodium cloud experiments have been discussed adequately in other sources [10, 11, 14, 18]. Observations show that large oscillations of horizontal velocity at vertical intervals of

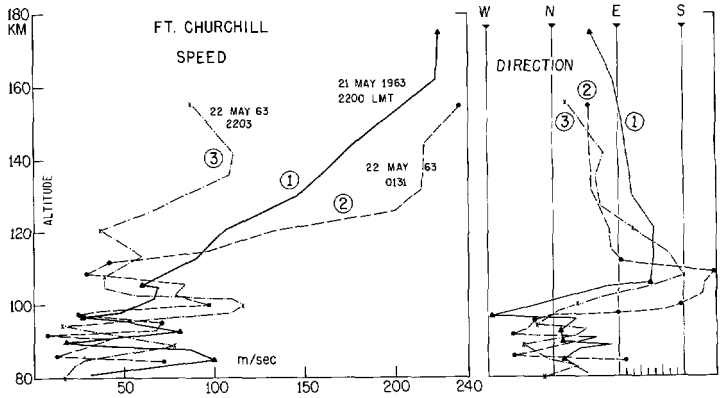

FIGURE 2.—Sodium cloud data from Fort Churchill with two soundings showing exceptionally high speed at heights 160–180 km. Note oscillatory character of velocity in the 80–120-km. region, identical with data from stations located in latitudes 30°– 40°N.

6–8 km. are always present up to 120 km. These oscillations attenuate at greater heights, leading to a "quiescent region" extending from 140 km. to at least 200 km.; in this region speed oscillations are not readily apparent, but may exist over vertical intervals greater than 40 or 50 km. Also observed in this region is a great constancy of wind direction for any given profile. Manring et al. [13] also found that their analysis of periodic motions, valid for the 85–135-km. region, was not applicable above 135 km., possibly because of a change in the character of the motion.

The data used in the present paper show a remarkable similarity among the winds from Wallops Island, Sardinia, and Eglin. This similarity suggests that within the 30°–40° N. latitude belt the motions are well organized and uniform. Little can be said about higher latitudes because only three soundings were available from Fort Churchill, two of them showing unusually strong motions. The data from Fort Churchill are illustrated in figure 2. The time interval between soundings No. 1 and No. 2 was 3½ hr.; between No. 2 and No. 3, 20½ hr. Up to 110 km., the speed profiles No. 1 and 2 conform to those of other stations, but at higher elevations they display a steady increase, reaching speeds of 240 m./sec. near 160 km. These strong motions were from the northeast, which is the usual direction of summer winds in this height region over Wallops Island and Sardinia.

An additional sounding from October 31, 1958 was available for Fort Churchill [1], and it indicated a wind of the same magnitude but at a lower height: the wind maximum was 255 m./sec. at 118 km., the wind direction 262°*. Comparing the strongest winds observed at other stations, it is found that they are well below the values measured at Fort Churchill: thus the absolute maximum in the whole sample for Wallops Island was 158 m./sec. (at 105 km.), for Sardinia 140 m./sec. (at 180 km.), and for Eglin 203 m./sec. (at 136 km.). It thus seems that,

*Throughout this paper the wind direction signifies that direction from which the air moves; e.g., an "easterly wind" is from the east and its direction is 090°.

even with due allowance for a small sample, the motions above 110 km. over Fort Churchill are much stronger than in latitudes 30°– 40° N.

The interpretation of figure 2 is not easy. We assumed wave motion existing through the whole depth of sounding No. 3, but ending at 110 km. in soundings No. 1 and 2. The upper portions of No. 1 and 2 would then be due to a combination of thermally controlled drift and tides. This assumption yields reasonable figures if checked by the thermal wind equation and by the mean temperatures. The shear vector between 110 and 160 km. is 68°/185 m./sec. in curve No. 1 and in curve No. 2, 39°/220 m./sec. On the assumption that all the motions are drift, this yields a horizontal temperature gradient in the north-south direction ($\partial T/\partial y$), of 120° K. per 10 deg. latitude at 110 km.; this value should be reduced by an unknown factor because of the presence of tidal components. A check by the hydrostatic relation yields a mean temperature for the 110–160-km. layer of 572° K., versus 622° K. for the mean temperature of the U.S. Standard Atmosphere 1962. Since the latter is an annual value, and the polar region in May should be, at least at 100–110 km., colder than in winter, the value of 572° K. seems reasonable.

The location of Fort Churchill in the auroral zone may have some connection with these extremely strong winds, but the relation is not obvious. It is found, for example, that the period May 15–22, 1963 contained only magnetically quiet days, with very low sunspot numbers, and without polar-cap absorption events that are manifestations of enhanced proton streams reaching the earth.

A summary of the observed winds at four locations is shown, in the form of the resultants, in figure 3. Above 140 km., the resultants represent fairly closely individual soundings. But in the 90–120-km. layer the magnitude of the resultants is about one-half of the average scalar wind speed. An outstanding similarity of motion is observed in the 80–120-km. layer in both summer and winter: westerlies prevailing in the lower portions of this layer change near 105 km. to northerlies, and then to easterlies. Even Fort Churchill, which reflects strong northeasterlies at 80–85 km., shows this change to northerlies at 90–95 km., with easterlies above 100 km. Other strong similarities appear in the 130–180-km. region. In summer, the flow in this region over all four stations is from the northeast or north-northeast, and the magnitude of this flow steadily increases with elevation. Strong speeds over Fort Churchill may, of course, be unrepresentative of seasonal averages. In winter, the region above 120 km. at Wallops Island and Eglin is occupied by uniform northwesterlies that also increase with elevation. In figure 3, the strongest resultant in each array is labeled with the appropriate speed in m./sec.

Of special interest is the distribution of the individual winds in the 140–200-km. region. Figure 4 illustrates all available winds from four stations, at height intervals of 10 km. Dashed brackets indicate range of directions for winter or summer; some extremely strong vectors are

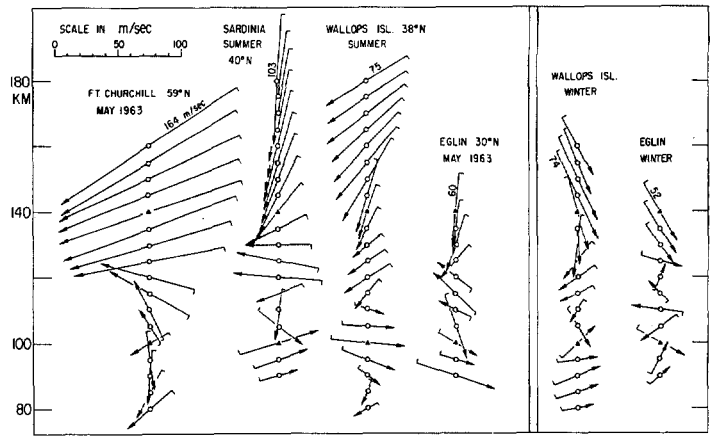

FIGURE 3.—Resultants of observed winds at four locations. From sodium cloud data. Strongest resultant in each array is labeled in m./sec.

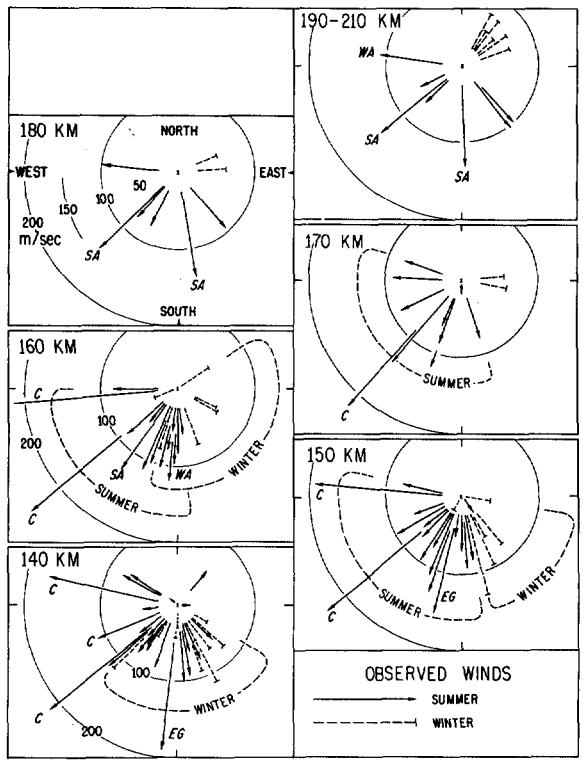

FIGURE 4.—Wind vectors from individual soundings at heights from 140 to 210 km. Data from Wallops Island, Sardinia, Eglin, and Fort Churchill. Note a pronounced lack of southerly component.

identified by C, SA, WA, and EG indicating that this particular wind was from Fort Churchill, Sardinia, Wallops Island, or Eglin respectively. A peculiar lack of southerly component is observed in the 140–180-km. region. A detailed check reveals that up to 115 km. the frequencies of the southerly and northerly components are about equal. However, in the 120–180 km. region the southerly component during winter appears in only 13 percent of the cases, with an average speed of 34 m./sec. versus

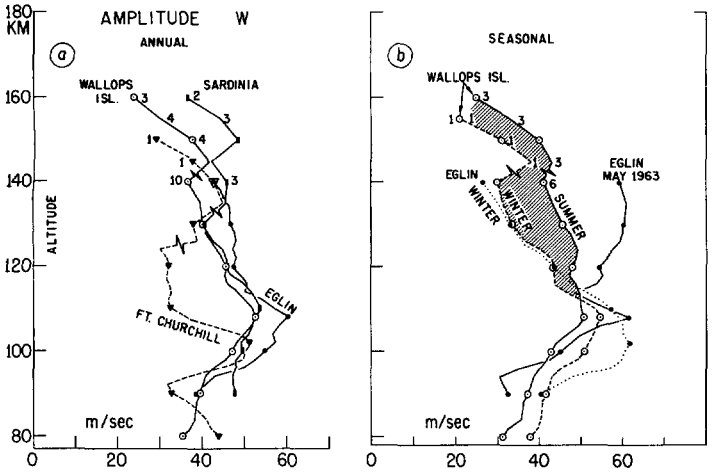

FIGURE 5.—Average magnitude of term W which is assumed to represent the amplitude of internal gravity waves. Near the top of the curves, number of available W profiles was small as shown by figures plotted near appropriate data points. Shading indicates the excess of summer values over winter data, for Wallops Island.

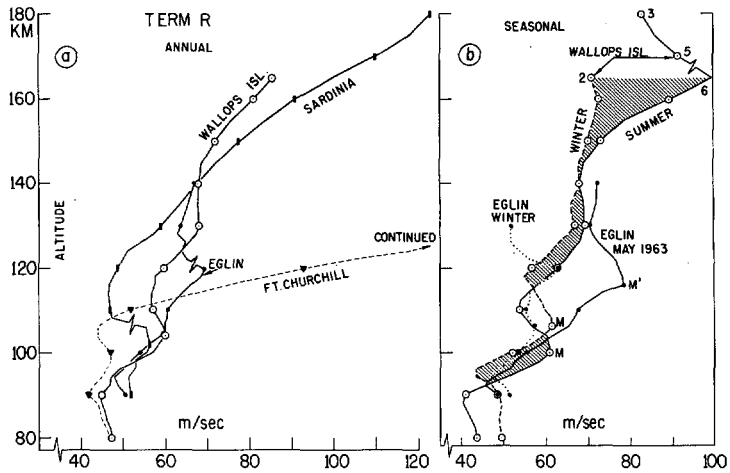

FIGURE 6.—Average magnitude of the residual term R. This term is assumed to be a sum of the prevailing wind and tidal components. The top part of curve for Fort Churchill is not shown, but it increases to 165 m./sec. at 140 km. and 181 m./sec. at 160 km. Shading indicates the excess of summer values over winter data, for Wallops Island.

47 m./sec. for the northerly component. In summer, the southerly component appears in 24 percent of cases, with speed of 31 m./sec. versus 45 m./sec. for the northerlies. No explanation is offered for this lack of southerlies but it should be noted that it implies a pole-to-equator circulation in the 120–180-km. region throughout the whole year. Near 200 km. the southerly component seems to reappear but only in winter.

5. MAGNITUDE OF WAVE MOTION AND RESIDUAL MOTION

The average amplitudes of the wave motion are shown in figure 5. Up to 130 km. all data were compiled at 2-km. intervals, and above 130 km. at 5-km. steps. Zigzag symbols were inserted in the curves wherever there was an obvious computational instability due to changing number of observations. Only a small number of cases was available in the topmost portions of the profiles, and they are shown by figures plotted near appropriate data points.

In figure 5a, the curves for Wallops Island, Sardinia, and Eglin display a remarkable similarity of shape. This suggests that within 30° – 40° N. latitudes the wave phenomenon is of the same character and intensity, with little or no longitudinal variation; the amplitudes rise from relatively low values at 80 km. to a peak near 108 km., and then decrease slowly with elevation. The lower part of Fort Churchill's curve conforms to the other stations, but too low values appear in the 105–125-km. layer; we interpret the latter as unrepresentative because of the small sample. Above 130 km., the W values from a single profile at Fort Churchill fit the general picture well.

Figure 5b indicates that the amplitude of gravity waves undergoes significant seasonal variations. The shaded portions show, for Wallops Island, the excess of summer values over winter data. It is seen that also at Eglin the amplitudes at all heights over 115 km. are much stronger in summer than in winter. It should be mentioned that, because of small data samples, our definitions of seasons are unconventional: (1) for Wallops Island, firings from April to September inclusive were grouped into "summer", those from November to March into "winter", (2) for Eglin, the "winter" data are from October, November, and December 1962, while the curve labeled "May 1963" includes only six soundings, four of them taken during the night of May 17, 1963.

The magnitude of the residual motion obtained from our vectorial resolution is shown in figure 6. This motion generally increases with elevation, and at heights over 120 km. steadily approaches the values of the observed wind.

The average annual magnitude of term R is represented in figure 6a. The curves for Wallops Island, Sardinia, and Eglin are again very similar. The upper part of Fort Churchill's curve is an exception and shows a very steep increase above 110 km.; in fact, the highest parts of this curve were omitted from figure 6a; it is sufficient to note that at 160 km. the value of R for this curve is 181 m./sec. The seasonal variations of R are shown in figure 6b, where shaded portions are again for Wallops Island and indicate the excess of summer values over winter data. At both Wallops Island and Eglin the summer values of R are generally stronger than the winter values. Thus, above 115 km. both R and W have the same seasonal trend.

In figure 6b some details call for further analysis. For example, on summer and winter profiles for Wallops Island two points labeled M (at 100 and 106 km.) are secondary maxima of R. They correspond to the "principal velocity

maximum" of the observed wind [10] that appears at 105 ± 5 km. On the Eglin curve labeled "May 1963" this maximum seems to be shifted upward to M′. The interpretation of this shift is uncertain; it could be a nighttime effect, or simply a spurious effect of a small sample.

The important inference from figures 5 and 6 is that above approximately 120 km. the share of the internal gravity waves in the observed motion decreases with elevation, while that of term R increases. The role of the gravity waves at greater heights may diminish even faster than hitherto indicated. Determining subjectively the presence of velocity oscillations in individual profiles, we find them in all soundings up to 120 km., but at greater heights their frequency of appearance seems to decrease substantially with elevation. While our method of determination of this feature is certainly questionable for greater heights, we feel that such a trend exists. The upper parts of some high-reaching soundings clearly show velocity oscillations, while in other profiles there are no oscillations over vertical intervals of 40 or 50 km. Thus unless the λ_z of the prevailing modes increases sharply with height, we may tentatively assume a decrease of the frequency of appearance of wave motion with elevation.

Figure 7 shows a summary of the findings discussed in this section. Curves labeled $\overline{V}$, $\overline{R}$, and W are in m./sec. and represent mean scalar values of the observed wind, the residual motion, and the amplitude of the wave motion. These curves are comprised of data from Wallops Island, Sardinia, and Eglin. Curve W has been extrapolated by a dashed line which was deliberately biased toward higher values, and this extrapolation suggests only a slight decrease of W with elevation. Curve F is the frequency of appearance of the wave motion; it indicates that up to 120 km. the wave motion appears in all profiles, dropping to 50 percent at 147 km. and to perhaps 9 percent at 180 km. Term $\overline{R}$ is, of course, present in 100 percent of cases at all elevations. Above 120 km. the speed of $\overline{R}$ is shown to approach gradually that of the observed wind. But even at lower heights there is surprisingly little difference between $\overline{R}$ and $\overline{V}$, indicating that $\overline{V}$ is insensitive to the removal of the oscillating component. Curve $W \times F$ is a product of amplitude and frequency of appearance of the wave motion, and represents an adjusted version of the upper part of curve W. The implications of this adjustment will be discussed in section 7.

A comparison of vectorial averages of the observed wind with those of **R** is presented in figure 8. All curves are for Wallops Island. Speed of the resultants is on the left, direction on the right. Also shown are annual values of the mean scalar speed (curves $\overline{V}$ and $\overline{R}$), where $\overline{R}$ trails closely behind $\overline{V}$. It is seen that the directions of the resultants for **V** and **R** are nearly identical, while the resultant speeds for **R** tend to be only slightly lower than those for **V**. It is also noted that between 100 and 135 km. the magnitude of the resultants is much smaller than the mean scalar speeds $\overline{V}$ or $\overline{R}$; in this region strong components of opposite sign have roughly equal frequency and tend to cancel each other, leaving weak resultants.

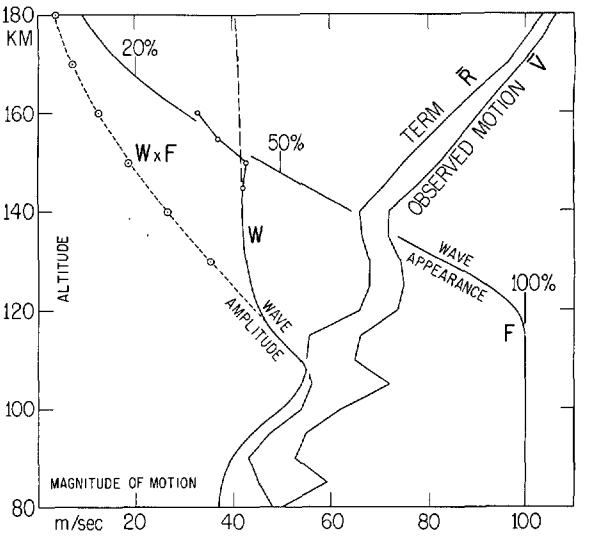

FIGURE 7.—Average magnitude of various types of motion in latitudes 30°–40° N. Combined data from Wallops Island, Sardinia, and Eglin. Curve $\overline{V}$ is mean scalar speed of the observed wind, $\overline{R}$ is mean speed of the residual term, W is amplitude of internal gravity waves, and F is frequency of appearance of wave motion. Curve $W \times F$ is an adjusted version of curve W, and accounts for gradual disappearance of internal gravity wave motion with elevation.

Further interpretation of the results shown in figure 8 leads to important conclusions regarding addition of periodic and nonperiodic motions. If such motions are combined, the averages of the total motion have properties which are not readily apparent. On a horizontal plane, a randomly distributed periodic motion disappears altogether from the vectorial averages. It affects the mean scalar speed of the total motion only if its magnitude exceeds one-half of the magnitude of the nonperiodic component. These relations can be illustrated on the following simplified model. Let us consider vector **OA** which is nearly invariant over, say, several days and represents a slowly varying prevailing wind. The mean scaler speed of this component is $\overline{OA}$. Observations of periodic motions (such as gravity waves) from twilight hours are assumed to be available. They can be represented by several vectors **AP** randomly distributed around point A. The vectorial mean of the combined motion is them simply $\widetilde{\mathbf{OA}}$, where contributions of the gravity waves have been eliminated. The mean scalar speed of the combined motion is $\overline{OP}$ and differs little from $\overline{OA}$ providing $OA > AP$. The approximate expression for the scalar speeds is then

$$\overline{OP}/\overline{OA} = 1 + 0.26(\mathbf{AP}/\mathbf{OA})^2$$

That is, if the magnitude of the periodic motion **AP** is ¾, ½, or ¼ of OA, the mean scalar speed of the combined motion is only 1.145, 1.065, and 1.016 of $\overline{OA}$, respectively.

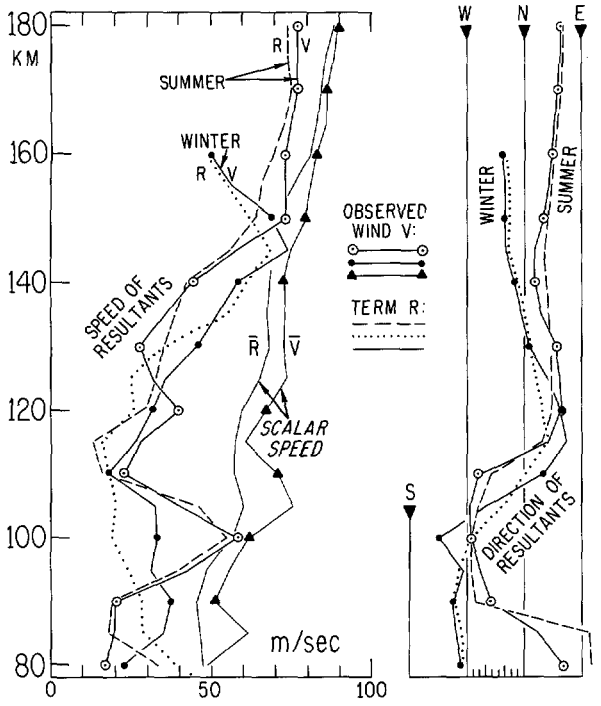

FIGURE 8.—Magnitude and direction of the resultants of observed wind, compared with the resultants of term **R**. Also shown are corresponding mean scalar speeds $\overline{V}$ and $\overline{R}$. Data from Wallops Island.

This explains, in part, why the averages of the observed wind are so insensitive to the removal of the oscillating component **W**. It also supplies some, if incomplete, interpretation of the residual term **R**: vectorial averages of **R** based on profiles from both a.m. and p.m. twilight hours eliminate contributions of the diurnal tide, and represent a sum of the prevailing drift and semidiurnal tide. Since the average contribution of the latter in the 30°–40° N. latitudes appears to be, at the most, 18 m./sec. in the 100–115-km. layer and 30 m./sec. at 160 km. (see table 5), the vectorial resultants of **R** represent, quite closely, those of the prevailing drift.

6. OTHER STATISTICS ON WAVE MOTION

Figure 9 shows frequency distributions of the magnitude of **W** (i.e., of the amplitude of internal gravity waves) for three stations. Data from all elevations between 80 and 170 km. were included, but the bulk of the data comes from the 90–140-km. layer. In figure 9, all cases in which W is equal to or greater than 70 m./sec. come from the 95–135-km. region. They amount to 12 percent of the total sample. The extreme value of W was 120 m./sec. with the corresponding R of 83 m./sec. at Eglin. Graphs for Wallops Island and Eglin suggest a non-peaked distribution for all values between 10 and 80 m./sec. The graph for Sardinia shows a peak in the 40–49 m./sec. class, but because of the small number of cases this peak is considered unrepresentative.

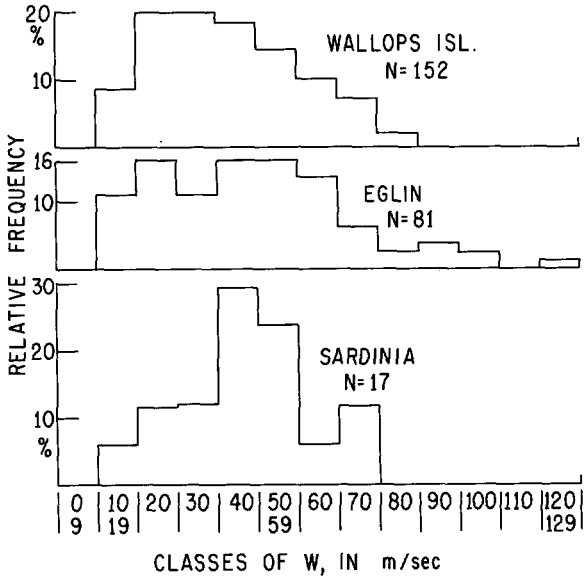

FIGURE 9.—Relative frequency of the magnitude of term W (i.e., of amplitude of internal gravity waves). Data from all heights between 80 and 180 km.

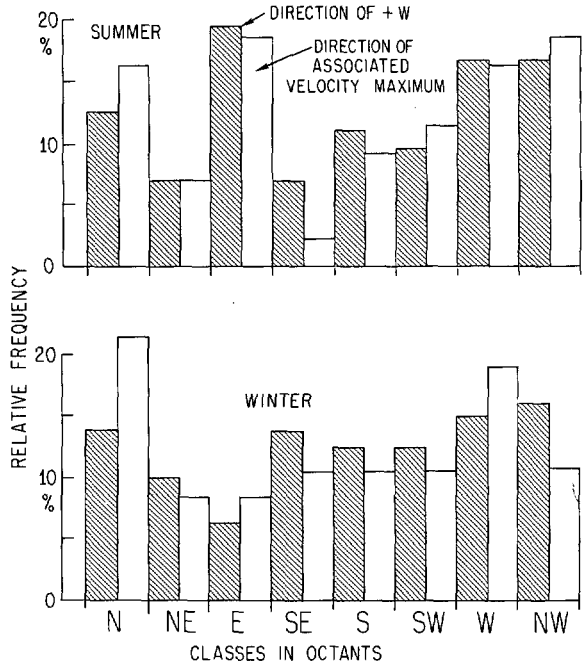

FIGURE 10.—Frequency of directions of vector $+\mathbf{W}$ (shaded blocks) and of the associated velocity maxima of the observed wind (open blocks).

The direction of the wave motion poses some interesting problems. Our vectorial resolution method requires the direction of vector $+\mathbf{W}$ to be generally close to the direction of the associated velocity maximum of the observed wind. This is confirmed by figure 10, which shows frequencies of directions for $+\mathbf{W}$ (shaded blocks) and for corresponding wind maxima (open blocks). The classes are in octants, where N encompasses directions from 338°

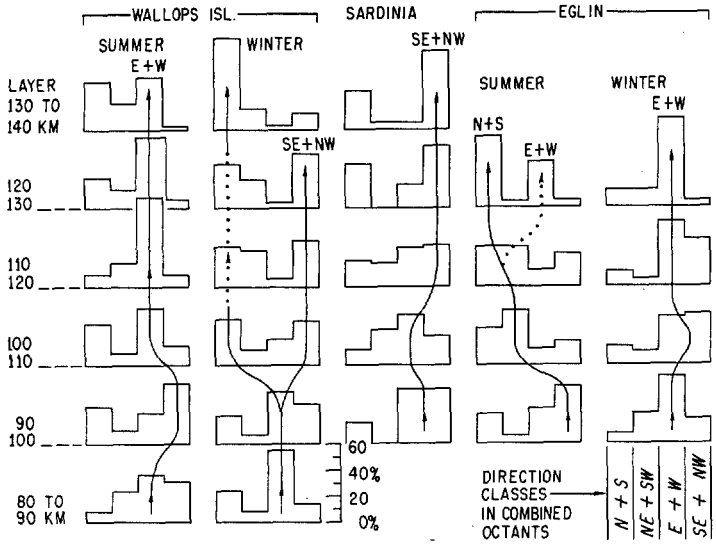

FIGURE 11.—Relative frequency of directions of wave vectors $+\mathbf{W}$ and $-\mathbf{W}$. Each class is for two opposing octants, because on individual soundings adjoining $+\mathbf{W}$ and $-\mathbf{W}$ always differ by 180°. Solid arrows indicate primary maxima of frequency, dashed arrows show some of the secondary maxima.

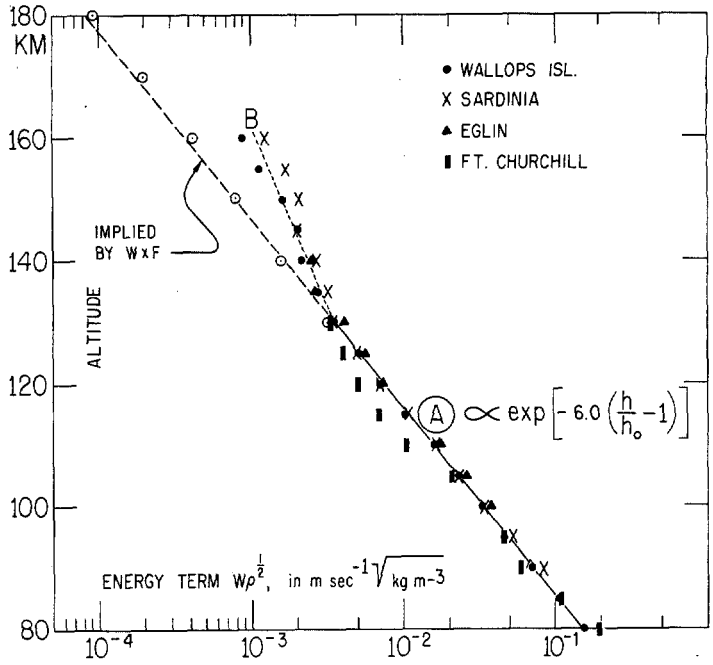

FIGURE 12.—Energy term of internal gravity waves. The equation applies to solid line A which is a fit to Wallops Island data from 80 to 130 km. Line B is a fit to all observational data in the 130–160-km. region. Open circles take into account the decrease of occurrence of wave motion with elevation and are based on curve $W \times F$ from figure 7.

to 22°, NE from 23° to 67°, etc. A nearly perfect agreement is obtained for summer data, and a less exact one for winter. It is also clear that parameter $+\mathbf{W}$ seems to have certain preferred directions: in summer, the greatest frequencies are found, in descending order, in octants E, W, and NW, where the sum for these three octants is 53 percent. In winter, the largest frequencies are in octants NW, W, and N, with a total of 45 percent. The vectorial resolution technique also implies that the direction of $+\mathbf{W}$ should be fairly close to that of $\mathbf{R}$; we find that in 94 percent of cases the direction of $+\mathbf{W}$ is within $\pm 60°$ of the direction of $\mathbf{R}$.

An analysis of wave directions by elevation is presented in figure 11. Directions of both $+\mathbf{W}$ and $-\mathbf{W}$ were counted and totaled for N+S octants, W+E octants, etc. The solid arrows in figure 11 show the maximum frequency, i.e. the most preferred alignments, while dotted arrows indicate secondary maxima of frequency. Above 90 km. the most preferred directions, in descending order, are W+E, SE+NW, and N+S. Figure 11 suggests that gravity waves may be polarized through deep layers, and that the direction of the polarization may change with season.

7. ENERGY CONSIDERATIONS

The decrease of the wave motion with elevation implies the dissipation of energy which will ultimately appear as heat and contribute to the dynamical heating of the upper atmosphere. As postulated by Hines, a system of internal gravity waves draws its energy from the stratosphere and propagates upward. If this system loses energy at some higher levels, appreciable heating will result. Hines [8] estimated that heating of the upper atmosphere from this source alone may amount to 10° K./day at 95 km., 30° K./day at 110 km. and about 100° K./day at 140 km. Comparable heating rates may be expected from the dissipation of tidal energy. In fact the steepest temperature increase throughout the whole upper atmosphere ($\partial T/\partial z$ of about 17° K./km.) found in the 120–160-km. region may be linked with the energy deposition from the lower atmosphere.

An exponential decrease of the wave motion energy in the 70–140-km. region was found in our earlier analysis [10]. More extensive sodium cloud data now permit expansion of these findings. The energy term for four stations is illustrated in figure 12, where it was chosen to show term $W\rho^{1/2}$ instead of the conventional $W^2\rho$. Density ρ (in kg./m.^{3}) was taken from the U.S. Standard Atmosphere 1962, and W from our derived data. The solid line A in figure 12 was drawn to Wallops Island data between 80 and 130 km. Values from other stations adhere well to this line except for four points from Fort Churchill at 110–125 km., where exceptionally low values of W resulted in a too small energy term. Dotted line B represents a fit to all data between 130 and 160 km. However, in this region it appears more appropriate to use values based on $W \times F$ which account for the gradual decrease of the frequency of appearance of wave motion

with elevation; these values are shown by open circles and fit well the upward extrapolation of line A.

The equations pertinent to figure 12 are:

Line A: $W\rho^{1/2} \propto \exp\left\{-6.0\left(\frac{h}{h_0}-1\right)\right\}$

for heights 80 to 180 km.

Line B: $W\rho^{1/2} \propto \exp\left\{-3.2\left(\frac{h}{h_0}-1\right)\right\}$

for heights 130 to 160 km.

Our earlier estimates of the rate of decrease of energy term were for the 70–140-km. region [10], but could be extended to the 80–180-km. layer. Such extension yields a factor of exp $-5.3[h/h_0-1]$, i.e., a slightly lower rate of energy dissipation than line A. However, the difference in the exponents is only 13 percent and at least a part of it is certainly due to the inaccuracy of drawing a best fit line.

8. SHORT-PERIOD VARIATIONS

Analyses of two nighttime series of chemoluminous trails by Rosenberg and Justus [20] suggest that velocity oscillations in the 90–150-km. region may be due to semidiurnal tides rather than to a non-tidal ensemble of internal gravity waves of 1–3-hr. period. While the theory (Hines [6], [8]) allows for modulation of gravity waves in their upward passage, by tides, presently available data are too few to draw definite conclusions. Using four observations from a 5½-hr. interval and another four from a 9-hr. interval, Rosenberg and Justus inferred horizontal wavelengths and periods that pointed to strong semidiurnal tides. In their interpretation, 90 percent of the variance of velocity oscillations of the order of 100 m./sec. would be accounted for by the 12-hr. tide, and the residual by the prevailing wind and 24-hr. tide.

Our vectorial resolution analysis applied to these two time-series yields a term **R** that seems to be dominated by the 12-hr. tide. Results regarding term **W** are inconclusive because in part they favor existence of long-period wave motion, but also point to oscillations of about 3-hr. to 4-hr. period. The analysis is questionable because the central portions of the two time series had observational gaps lasting 5 and 4 hr., for which smoothed interpolation given by Rosenberg and Edwards [19] was accepted. Time cross-sections of the observed data (not reproduced) show alternate layers of easterly and westerly components superimposed on each other; similar layers appear in northerly and southerly components. These layers are inclined downward, as if wind patterns were descending to lower levels at the rate of 0.9 m./sec. during the May 1963 series, and 0.4 m./sec. during the December 1962 series.

The derived patterns of **W** and **R** for the night of May 17, 1963 are shown in figure 13. The distribution of firings is indicated by the vertical dashed lines in figure 13c.

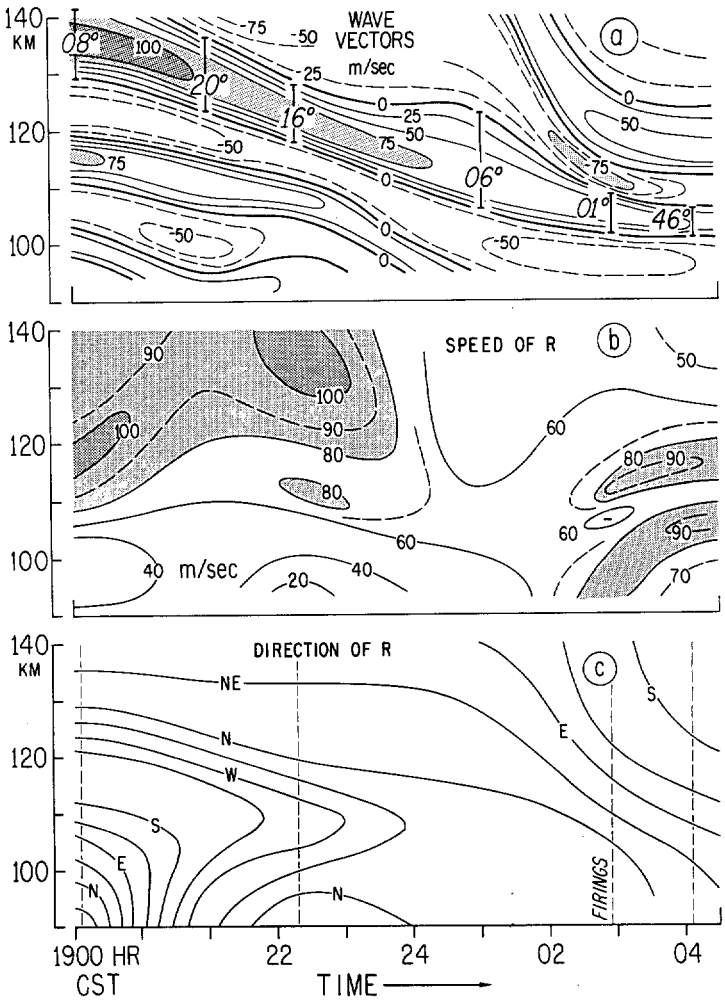

FIGURE 13.—Derived quantities from four closely spaced experiments at Eglin, the night of May 17–18, 1963. Distribution of firings is shown on figure 13c by dashed vertical lines. In figure 13a the isotachs represent the magnitude of vectors of internal gravity waves, positive values (solid lines) adding to the residual motion **R**, and negative values (dashed lines) subtracting from it. The directions of vector $+\mathbf{W}$ for one strong wave system are shown by slant figures.

As suggested by figure 13a, the wave motion had a strong system where the amplitude **W** exceeds 100 m./sec. (stippled portions). This system progresses downward at an average rate of 1 m./sec.; in layers marked by vertical bars the directions of $+\mathbf{W}$ are indicated by slant figures which suggest that in general, this system preserves its direction.

There are other systems, not nearly as regular however. In these systems, at a given horizontal level the directions of $+\mathbf{W}$ are highly variable. At 108 km., for example, the profiles from 1906 and 2100 CST have the $+\mathbf{W}$ directions of 21° and 208°, i.e., the direction difference is close to 180°. This can be interpreted as due to a gravity wave with a period of about 4 hr. Firings from 0255 and 0406 CST have the $+\mathbf{W}$ directions of 314° and 196° (i.e., a difference of 118°), suggesting a wave with a

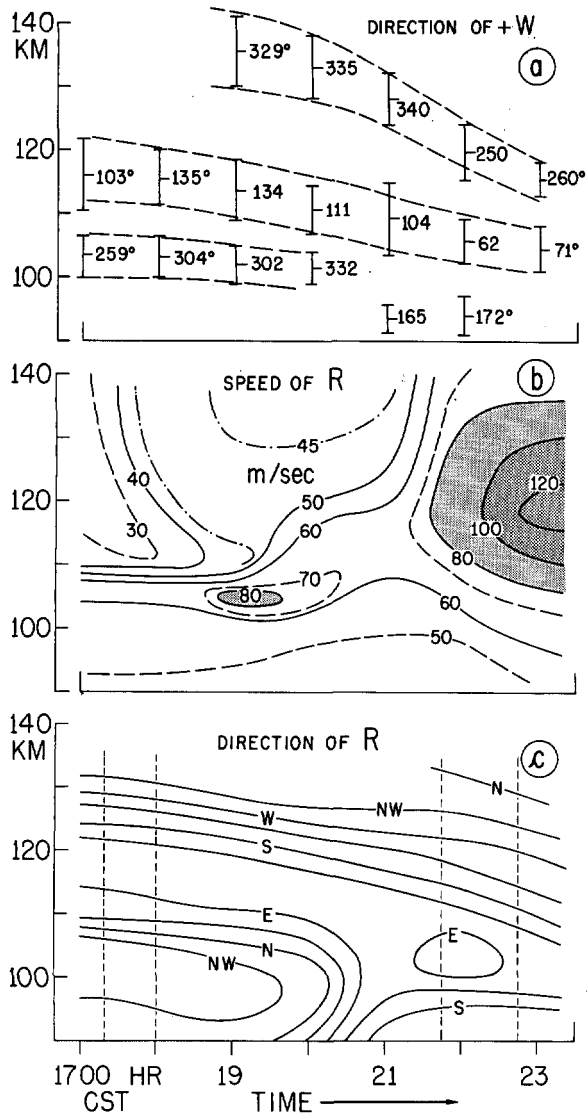

FIGURE 14.—Derived quantities from four closely spaced experiments at Eglin, the evening of December 3, 1962. Distribution of firings is shown on figure 14c by dashed vertical lines.

period of 3 hr. The speed of term **R** (fig. 13b) also shows a strong system, presumably dominated by the 12-hr. tide. The evidence for the latter comes from figure 13c, which depicts the direction of term **R**; at levels from 100 to 125 km. the changes of direction over 9 hr. are nearly 360°, but at 130–140 km. these changes are close to 180°. Along the vertical, vector **R** shows a clockwise rotation as required by the theory of tides.

The derived motions for the night of December 3, 1962 are shown in figure 14. There were three fairly strong wave systems and the directions of $+\mathbf{W}$ for these systems are shown in figure 14a. The middle system seems to have a remarkable stability of direction over at least a 6-hr. period, while other systems show stability over 2–3-hr. intervals. However, the observational gap between 1800 and 2145 CST makes this analysis doubtful. The only really certain data are for the 41-min. period at the beginning of this series, and for the 60-min. period at the end of it. They indicate small direction changes between the first and second firings, and also between the third and fourth firings, suggesting that if short-period oscillations were present, their amplitude was quite small.

The middle system in figure 14a indicates a downward progression of 0.6 m./sec., the topmost system 1.4 m./sec. The speed of **R** (fig. 14b) at heights over 110 km. changes substantially in 6 hr., as does its direction (fig. 14c). The latter shows again a clockwise rotation with elevation. Reading 6-hr. direction changes from figure 14c and extrapolating them to 12 hr., one finds a 360° change in the 100–120-km. layer, and a 180° change in the 125–130-km. layer. In general, term **R** in figures 13 and 14 suggests the presence of considerable semidiurnal tide in addition to appreciable short-period gravity waves.

9. TIDAL MOTIONS

Most of the chemoluminous cloud observations are limited to twilight hours and conventional harmonic analysis cannot be applied to these data. Yet information about tides and the general circulation above 100 km. would be of great importance for understanding processes occurring in the lower thermosphere.

Our residual term **R** presumably contains components due to diurnal and semi-diurnal tides, as well as thermally controlled drift. Term **R** can be resolved to give the component of the diurnal tide at approximately 6 p.m. and 6 a.m. Only a slight assumption is needed, viz., that all soundings from the evening twilight hours apply to 6 p.m., and those from the morning twilight to 6 a.m. The method is similar to that previously used and can be illustrated by assigning new definitions to figure 1. In the top part of figure 1, let vector $\mathbf{V_A}$ represent the vectorial mean of our residual term at 6 a.m. and vector $\mathbf{V_B}$ the residual term at 6 p.m. Then, vector $+\mathbf{W}$ is the component of the 24-hr. tide at 6 a.m. and $-\mathbf{W}$ at 6 p.m. Vector **R** in figure 1 becomes the remaining motion that occurs between 6 a.m. and 6 p.m. and contains the prevailing drift and semidiurnal tide.

This analysis was carried out on 28 profiles (23 from Wallops Island and 5 from Sardinia) and results are shown in figure 15. For the 24-hr. tide the 6 a.m. components are given; the 6 p.m. components are of the same magnitude but differ by 180° in direction. All points on figure 15 are to be read as indicated by the dashed arrow drawn to the point representing the height of 105 km.: at this height the component of the 24-hr. tide at 6 a.m. is 159°/22 m./sec. It should be emphasized that the amplitudes of the 24-hr. tide will generally be greater than the 6 a.m. components shown in figure 15. Another characteristic of the hodograph curve for the 24-hr. tidal components is a clockwise rotation in the 80–120-km. region, as required by tidal theory. No change is indicated in the 120–140-km. region. At heights from 140 to 160 km. the curve shows little rotation and goes near zero values, as if it no longer represented tidal phenomena. The second curve in figure 15 depicts the sum of the prevailing drift and the

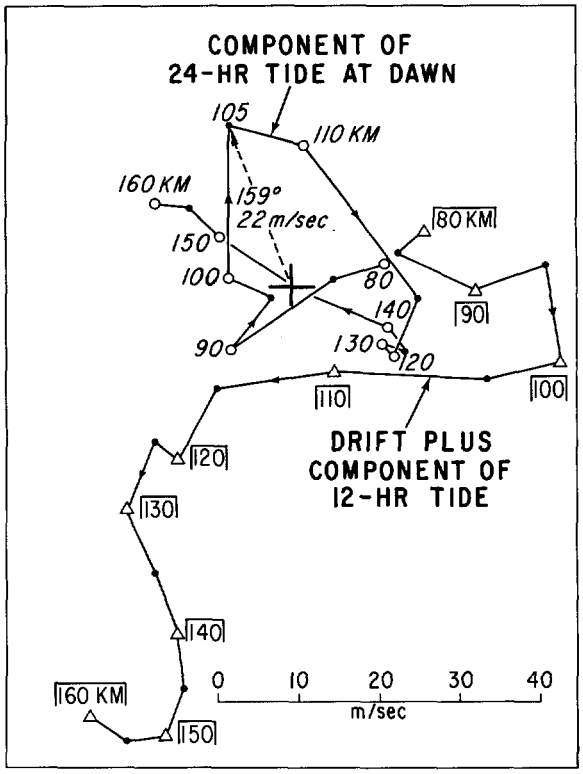

FIGURE 15.—Upper curve shows components of the diurnal tide at dawn, at elevations from 80 to 160 km. The lower curve represents the sum of the prevailing drift plus semidiurnal tide around midnight. Derived from 6 a.m. and 6 p.m. data for Wallops Island and Sardinia (28 soundings from nearly all months of the year).

semidiurnal tide. This sum is generally stronger than the 24-hr. tidal components, much so at heights greater than 130 km.

For the 90–130-km. region a very similar picture has been obtained by Hines [9], who used averages of the total observed wind from sodium cloud drifts over Wallops Island. The magnitudes of tidal vectors derived by Hines [9] are, on the whole, larger by a factor of 1.3 than those shown in figure 15, as if they included a contribution from a gravity wave component; Hines also found the maximum of tidal component in the vertical appearing at 105 km., and in his data the vector was 161°/40 m./sec.

10. INFERENCES FROM IONOSPHERIC DATA

Further information about prevailing drift and tidal motions can be obtained from ionospheric data but only in the form of qualified estimates. In many measurements of ionospheric movements, the question of whether they represent mass motions or phase progression remains unanswered. In the F region the relation between the motion of the ionized component and that of the neutral component is completely unknown. It is generally agreed, however, that at least in the lower E region the ionized component has little independent mass-motion

TABLE 1.—*Drifts of ionospheric irregularities compared with sodium cloud winds.* $\overline{V}$ *is the* observed *mean scalar speed for both categories.* $\mathbf{S}_r$ *are resultant vectors of ionospheric "steady component", and* $\mathbf{R}_r$ *represents resultant vectors of term* **R** *derived from sodium cloud winds. All speeds in m/sec. Ionospheric data from Rao and Rao [15, 16].*

(A) APPARENT IONOSPHERIC MOVEMENTS

Station	Latitude	E region		$F2$ region	
		$\overline{V}$	$\mathbf{S}_r$	$\overline{V}$	$\mathbf{S}_r$
Gorky	56° N	—	—	97	ESE 25
De Bilt	52° N	90	SSE 07*	—	—
Simeiz	44° N	—	—	115	E 11*
Ashkabad	38° N	—	—	74	N 41
Yamagawa	31° N	78	WNW 52	80	NW 50
Waltair	18° N	86	NNW 23	100	WSW 26
Wellington	41° S	80	WSW 29	—	—

(B) SODIUM DRIFTS

Station	Latitude	100–115 km.		155–160 km.	
		$\overline{V}$	$\mathbf{R}_r$	$\overline{V}$	$\mathbf{R}_r$
Ft. Churchill	59° N	75	ESE 41	—	—
Sardinia	40° N	66	NNE 39	95	NNE 85
Wallops Isl.	38° N	69	NNW 26	82	N 60
Eglin	30° N	77	ENE 23	72°	—

*Too low, probably because of cancellation of components of opposite sign.
°= Extrapolated.

TABLE 2.—*Resultant vectors of total observed motion at 6 a.m. and 6 p.m., and means of 6 a.m. + 6 p.m. values. Figures show direction of the resultant vectors in degrees, and their magnitude in m./sec. (in italics). Data for Yamagawa are for apparent ionospheric movements in the E region and represent vector sum of "steady component",* $\mathbf{S}_r$*, plus vectors of 24-hr. and 12-hr. periodic components. Data for Wallops Island and Eglin are for 100–115-km. layer and represent residual term* **R** *from sodium cloud drifts. Ionospheric values adapted from Rao and Rao [16].*

	SUMMER			WINTER		
	6 a.m.	6 p.m.	6 a.m. + 6 p.m.	6 a.m.	6 p.m.	6 a.m. + 6 p.m.
Yamagawa	273°	276°	275°	040°	088°	068°
	31	*47*	*39*	*25*	*32*	*26*
Wallops Isl.	267°	315°	290°	359°	041°	021°
	25	*26*	*23*	*29*	*29*	*26*
Eglin	069°	296°	055°	356°	077°	026°
	44	*14*	*18*	*36*	*23*	*25*

and that it is carried by the moving neutral component. We shall assume that the apparent movements of ionospheric irregularities in the E region, observed at a frequency of 2 megacycles/sec. are in this category. Rao and Rao [16] subjected data on these apparent movements to harmonic analysis, and isolated 24-hr. and 12-hr. periodic variations and a steady drift $\mathbf{S}_r$, where the subscript r indicates that S is a resultant vector. In the material from seven stations, all three terms revealed large but non-systematic latitudinal variations. They also studied ionospheric movements in the $F2$ region [15]. In neither study was the height of the observed phenomena stated by the authors, but we shall assume that for the E region this height was 100–115 km., and for the $F2$ region 150–250 km.

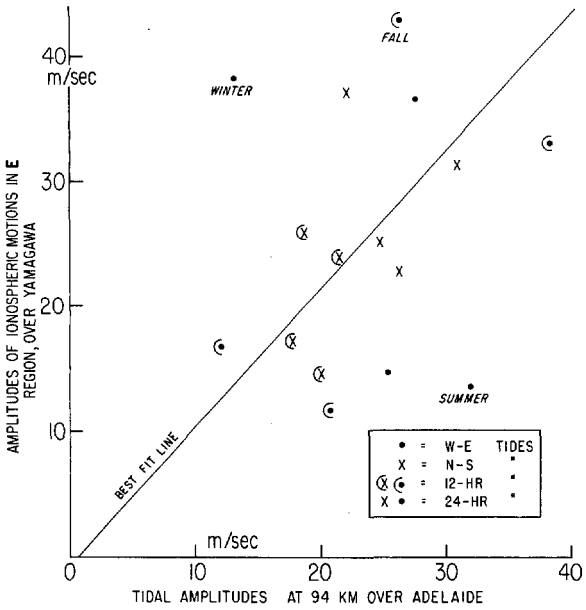

FIGURE 16.—Comparison between amplitudes of atmospheric tides at Adelaide (35° S., 138° E.) and amplitudes of 24-hr. and 12-hr. periodic terms from apparent movements of ionospheric irregularities in the E region over Yamagawa (31° N., 131° E.). Points represent seasonal values for conventionally defined seasons (where, e.g., "Summer" includes data from June, July, and August for Yamagawa, and from December, January, and February for Adelaide).

Let us examine first the mean scalar speed and the steady component of the ionospheric movements. The annual values for these parameters are shown in Table 1 (A). Table 1 (B) gives data from sodium cloud drifts, where $\overline{V}$ is the mean scalar speed of the observed wind and $\mathbf{R}_r$ is the annual resultant of the residual term $\mathbf{R}$.

As far as heights are concerned, strict comparison between sodium cloud data and ionospheric data is possible only for the E region; it must be kept in mind that sodium winds at 155–160 km. shown in table 1 (B) are from the very bottom of the F region. As indicated by table 1, there is a close similarity between ionospheric movements and sodium drifts in the E region. Even in the $F2$ region ionospheric scalar speeds $\overline{V}$ are about the same as wind speeds at 155–160 km., but magnitudes of $\mathbf{S}_r$ are significantly smaller than those of $\mathbf{R}_r$.

Periodic components from ionospheric data may well represent actual tidal motions. This is suggested by the comparison given in table 2. Yamagawa (31° N., 131° E.) was chosen for this comparison because its latitude is closest to that of Wallops Island and Eglin. In table 2, total ionospheric drift at 6 a.m. or 6 p.m. was obtained by combining $\mathbf{S}_r$ with the vectors of 24-hr. and 12-hr. harmonics. Values for Wallops Island and Eglin are resultants of term $\mathbf{R}$. Data for Yamagawa are from conventional three-month seasons, those for Wallops Island and Eglin from arbitrarily defined "seasons." Considering

TABLE 3.—*Magnitude of apparent ionospheric movements, in m./sec. Each value is an average of four seasonal means. Data for Yamagawa are in italics. Adapted from Rao and Rao [15, 16].*

	Scalar speed $\overline{V}$	Steady drift $\mathbf{S}_r$	Amplitudes of periodic motions			
			A_{24}		A_{12}	
			W-E	N-S	W-E	N-S
Yamagawa, E region	*76*	*39*	*26*	*29*	*26*	*20*
Yamagawa, $F2$ region	*80*	*37*	*24*	*23*	*16*	*20*
Waltair, E region	84	24	80	30	12	40
Waltair, $F2$ region	96	15	84	75	20	25
Ashkabad, $F2$ region	74	34	13	11	35	13
Gorky, $F2$ region	99	40	28	21	34	26

this and other uncertainties, ionospheric and wind data in table 2 show fairly close similarities. Eglin values in summer do not conform to those at the other stations, probably because of the unrepresentative sample (only six nighttime soundings from May 1963). In winter, values for Eglin and Wallops Island are very similar, but depart by about 40° from the vectors for Yamagawa. The mean scalar speeds for the data shown in table 2 are, for ionospheric drifts 68 and 67 m./sec., and for sodium winds 71 and 66 m./sec., for summer and winter respectively.

Periodic components of ionospheric movements in the E region also approximate the magnitude of tidal motions derived from meteor winds. Figure 16 compares tidal amplitudes over Adelaide [4] with amplitudes of 24-hr. and 12-hr. harmonics at Yamagawa. Considering the very short data periods on which the values for Adelaide and Yamagawa were based, the agreement is very close. Except for three points labeled "winter," "fall," and "summer," a good correlation exists between the two sets of data. The best fit line indicates a nearly 1:1 relation, ionospheric amplitudes being slightly stronger than those of real tidal motions. From comparison of the phases of the two sets (not reproduced) it is found that for the 24-hr. harmonics the differences are less than 6 hr. in 38 percent of the cases, and for the 12-hr. harmonics less than 3 hr. in 50 percent of the cases.

Several inferences can be drawn from this analysis regarding the E region:

(1) At heights of 100–115 km. the motions of neutral and ionized components appear to be quite similar.

(2) Appreciable periodic variations detected in apparent ionospheric movements are probably due to tides. Data for Yamagawa imply tides of amplitude 20–30 m./sec. and a prevailing drift of 40 m./sec.

(3) Ionospheric data suggest that the amplitudes of 24-hr. and 12-hr. tides are about the same, with slight preponderance of the former.

Similar results were obtained by Roper and Elford [17], who applied spectrum analysis to sodium cloud data up to 97 km. and found that spectral peaks for 24 and 12 hr. are roughly equal.

In the $F2$ region, the apparent ionospheric movements

TABLE 4.—*Various components of motion, in m./sec. Values implied from ionospheric drifts are in italics. Data for Adelaide and Jodrell Bank are from radio meteor winds, for Wallops Island from sodium trails.*

	Scalar speed $\overline{V}$	Term R: speed $\overline{R}$	Term R: resultant $\mathbf{R}_r$	Drift: resultant $\mathbf{D}_r$	Amplitudes of tides A_{24}	Amplitudes of tides A_{12}
Wallops Isl., 100–115 km	69	59	26	*30*	*21*	*18*
Adelaide, 95 km				21	18	9
Jodrell Bank, 92 km				12	*5*	10
Wallops Isl., 160 km	83	81	60	*37*	*19*	*30*

TABLE 5.—*Estimates of the magnitude of various types of motion in latitudes 30°–40° N. All values in m./sec.*

	Height region 100–115 km.	Height region 155–160 km.
Observed motion, scalar speed $\overline{V}$	67	90
Prevailing drift, scalar speed $\overline{D}$	45	65
Wave motion, amplitude W	50	40
24-hr. tides, amplitude A_{24}	21	20
12-hr. tides, amplitude A_{12}	18	30

cannot be safely interpreted as mass-motions. Nevertheless, the possibility that the periodic components represent tides and the steady components depict drift, should not be ruled out entirely. We shall assume that this possibility exists, simply as a hypothesis-for-argument, and examine the inferences. A comparison between the E region and the $F2$ region indicates that ionospheric periodic and steady components change little in intensity. This is illustrated in table 3 by data for Yamagawa (31° N.), where A_{24} and A_{12} represent amplitudes of the 24-hr. and 12-hr. periodic motions respectively, for the W–E and N–S components. For Yamagawa the values of A_{24} and A_{12} in the $F2$ region are slightly lower than those in the E region, suggesting a very slight attenuation of tides with height. In data presented by Rao and Rao [15, 16], the only other station permitting comparison between E and $F2$ regions is Waltair (18° N.). This station is different from all others in that it shows exceptionally strong 24-hr. harmonics, which may be a feature of the equatorial region. The last two rows in table 3 indicate values for the $F2$ region at Ashkabad (38° N.) and Gorky (56° N.). They suggest that 12-hr. periodic motions are stronger than 24-hr. motions, while the opposite is indicated for the $F2$ layer over Yamagawa. Without going into this and other uncertainties shown by the ionospheric data, we accepted Yamagawa, Ashkabad, and Gorky as representative for the $F2$ region in middle latitudes; the means for these three stations still show that A_{12} is greater than A_{24}.

Table 3 affords a tool for estimating the magnitude of slowly varying drift and tidal components that are hidden in sodium cloud data. Using values from table 3 and forming ratios $\mathbf{S}_r/\overline{V}$, $A_{24}/\overline{V}$, and $A_{12}/\overline{V}$ we can apply these ratios to sodium cloud winds, by taking for $\overline{V}$ the mean scalar speed of the observed wind. Values so obtained are shown in italics in table 4. In the E region the derived tidal amplitudes compare well with the observed tides at Adelaide. The value of 21 m./sec. for A_{24} is also in agreement with our figure 15 where tidal components at 6 a.m. average 16 m./sec. for the 100–115-km. region. The derived drift resultant of 30 m./sec. in table 4 seems to be much too high; it should be lower than R_r, and lower than 23 m./sec. which is the residual term from figure 15. At 160 km. the derived values in table 4 are doubtful indeed because they were obtained from the ratios of ionization drifts valid for the $F2$ region. They show a somewhat low value for $\mathbf{D}_r$ and imply an increase of the semidiurnal tide with elevation. We can also estimate from table 4 the mean scalar speed of the prevailing drift, i.e., $\overline{D}$. Sodium cloud data show that in the 100–115-km. layer the ratios $\mathbf{V}_r/\overline{V}$ and $\mathbf{R}_r/\overline{R}$ are 0.47. Assuming that the same relationship holds for $\mathbf{D}_r/\overline{D}$ and scaling $\mathbf{D}_r$ down to 21 m./sec., we obtain $\overline{D}$ of 45 m./sec. At 155–160 km. this ratio is 0.77 and for $\mathbf{D}_r$ of 40 m./sec., the value of $\overline{D}$ would be 52 m./sec. Table 4, incidentally, points out the desirability of having ionospheric and sodium cloud experiments performed at the same locations; with sodium cloud trails occasionally reaching 200 km., much can be gained in these two fields by simultaneous and side-by-side observations.

11. ESTIMATES OF VARIOUS TYPES OF MOTION

Table 5 is an attempt to summarize the scalar magnitudes of various types of motion that contribute to total wind observed at 100–115 km. and at 160 km. Only the first row represents the observed data. All other entries are derived values and represent tentative estimates subject to substantial changes. The first two rows of table 5 show the mean scalar speed. The last three rows are amplitudes of the oscillating and periodic components. In the case of motion due to internal gravity waves, its average contribution to the observed movements at a horizontal plane would be 1.16 $(2W/\pi)$, as indicated in section 3. Contributions from tides are probably close to $[(A_{24})^2+(A_{12})^2]^{1/2}$.

It is obvious that the estimates shown in table 5, particularly of drift $\overline{D}$ and of tidal amplitudes, are highly uncertain, and that other combinations are possible that would yield the observed values of $\overline{V}$. For example, a portion of our oscillating component may in reality represent tides, calling for a decrease of W, and an increase of tidal amplitudes; in particular, our estimates of semidiurnal tides may be too low, but it is doubtful that the amplitude of these tides in the whole E region would be 50 m./sec., as suggested by limited nighttime series from Eglin. With the possibility that semidiurnal tides may be stronger than shown in table 5, and with the evidence of appreciable diurnal tides, the estimates of the magnitudes of $\overline{D}$ and W may need to be revised down. On

the whole, however, we tend to favor the idea that prevailing drift is one of the major contributors to the observed motion.

In interpreting $\overline{V}$ and $\overline{D}$ values from table 5, care must be taken when converting these values to resultants, i.e., to $|\mathbf{V}_r|$ and $|\mathbf{D}_r|$. In the 100–120-km. layer the resultants are much weaker than corresponding mean scalar speeds, the observed ratios of $\mathbf{V}_r/\overline{V}$ and of $\mathbf{R}_r/\overline{R}$ being 68, 53, 30, 35, and 50 percent at heights of 100, 105, 110, 115, and 120 km. respectively. At 155 and 160 km. this ratio is 77 percent.

ACKNOWLEDGMENTS

The research reported in this paper has been supported by grants from the Atomic Energy Commission and National Science Foundation.

REFERENCES

1. J. E. Ainsworth, D. F. Fox, and H. E. LaGow, "Measurements of Upper-Atomosphere Structure by Means of the Pitot-Static Tube," *NASA Technical Note* D–670, Washington, D.C., Feb. 1961.
2. J. E. Blamont and J. M. Baguette, "Quelques résultats déduits de l'étude de la déformation de nuages artificiels de métaux alcalins," *Comptes Rendus de l'Académie des Sciences*, vol. 252, 1961, pp. 3099–3101.
3. L. Broglio, "Review of Italian Meteorological Activities and Results," *Proceedings of the First International Symposium on Rocket and Satellite Meteorology*, H. Wexler and J. E. Caskey, Jr. editors, North-Holland Publishing Co., Amsterdam, 1963, pp. 94–118.
4. W. G. Elford, "A Study of Winds between 80 and 100 km in Medium Latitudes," *Planetary and Space Science*, vol. 1, 1959, pp. 94–101.
5. Geophysics Corporation of America, "Experimental Study on the Dynamics and Structure of the Upper Atmosphere," *GCA Technical Report* No. 64–10–N, Contract No. NASw–712, Bedford, Mass., June 1964.
6. C. O. Hines, "Internal Atmospheric Gravity Waves at Ionospheric Heights," *Canadian Journal of Physics*, vol. 38, 1960, pp. 1441–1481.
7. C. O. Hines, "Minimum Vertical Scale Sizes in the Wind Structure above 100 Kilometers," *Journal of Geophysical Research*, vol. 69, No. 13, July 1964, pp. 2847–2848.
8. C. O. Hines, "Dynamical Heating of the Upper Atmosphere," *Journal of Geophysical Research*, vol. 70, No. 1, Jan. 1, 1965, pp. 177–183.
9. C. O. Hines, "Diurnal Tide in the Upper Atmosphere," *Journal of Geophysical Research*, vol. 71, No. 5, Mar. 1, 1966, pp. 1453 1459.
10. A. Kochanski, "Atmospheric Motions from Sodium Cloud Drifts," *Journal of Geophysical Research*, vol. 69, No. 17, Sept. 1, 1964, pp. 3651–3662.
11. A. Kochanski, "Atmospheric Phenomena in the Height Region from 70 to 160 km," in "The Circulation in the Stratosphere, Mesosphere, and Lower Thermosphere," R. J. Murgatroyd, ed., *WMO Technical Note*, No. 70, World Meteorological Organization, Geneva, 1965.
12. E. Manring, J. F. Bedinger, and H. B. Pettit, "Some Wind Determinations in the Upper Atmosphere Using Artificially Generated Sodium Clouds," *Journal of Geophysical Research*, vol. 64, No. 6, June 1959, pp. 587–591.
13. E. Manring, J. Bedinger, H. Knaflich, and D. Layzer, "An Experimentally Determined Model for the Periodic Character of Winds from 85 to 135 km," *GCA Technical Report* 63–27–N, Geophysics Corp. of America, Nov. 1963.
14. E. Manring, J. Bedinger, H. Knaflich, and D. Layzer, "An Experimentally Determined Model for the Periodic Character of Winds from 85 to 135 km," *NASA Contract Report* CR–36, Washington, D.C., July 1964.
15. G. L. Rao and B. R. Rao, "World Wide Study of Apparent Horizontal Movements in F2-Region of the Ionosphere," *Journal of Atmospheric and Terrestrial Physics*, vol. 26, 1964, pp. 213–229.
16. G. L. Rao and B. R. Rao, "The Latitude Variation of Apparent Horizontal Movements in the E Region of the Ionosphere," *Journal of Geophysical Research*, vol. 70, No. 3, Feb. 1, 1965, pp. 667–677.
17. R. G. Roper and W. G. Elford, "Periodic Wind Components at Meteor Heights," *NASA Technical Note* X–650–65–86, Goddard Space Flight Center, March 1965.
18. N. W. Rosenberg, editor, "Project Firefly 1962–1963," *Environmental Research Paper* No. 15, Air Force Cambridge Research Laboratories, May 1964.
19. N. W. Rosenberg and H. D. Edwards, "Observations of Ionospheric Wind Patterns through the Night," *Journal of Geophysical Research*, vol. 69, No. 13, July 1, 1964, pp. 2819–2826.
20. N. W. Rosenberg and C. G. Justus, "Space and Time Correlations of Ionospheric Winds," *Radio Science*, vol. 1 (New Series), No. 2, Feb. 1966, pp. 149–155.

[*Manuscript received September 27, 1965; revised December 30, 1965*]